

# Evolution of fundamental parameters in emission line galaxies up to $z \sim 0.4$

M. A. Lara-López<sup>1,2</sup>, J. Cepa<sup>1,2</sup>, A. Bongiovanni<sup>1,2</sup>, A. M. Pérez García<sup>1,2</sup>,  
A. Ederoclite<sup>1,2</sup>, H. Castañeda<sup>3</sup>, M. Fernández Lorenzo<sup>1,2</sup>, M. Pović<sup>1,2</sup>, and  
M. Sánchez-Portal<sup>4</sup>

<sup>1</sup> Instituto de Astrofísica de Canarias, 38200 La Laguna, Spain

<sup>2</sup> Departamento de Astrofísica, Universidad de la Laguna, Spain

<sup>3</sup> Departamento de Física, Escuela Superior de Física y Matemática, IPN, México D.F., México

<sup>4</sup> Herschel Science Center, INSA/ESAC, Madrid, Spain

## Abstract

In this work we focus on the evolution of the SFR, metallicity of the gas, and morphology of galaxies at low redshift in search of signs of evolution. We analyzed the evolution of the SFR, metallicity, and morphology, through the mass–metallicity, luminosity–metallicity, SFR–stellar mass, and SFR–metallicity relationships of star–forming galaxies from SDSS–DR5 (Sloan Digital Sky Survey–Data Release 5), using redshift intervals in bins of 0.1 from  $\sim 0$  to 0.4. We used data processed with the STARLIGHT spectral synthesis code, correcting the fluxes for dust extinction, and estimating metallicities using the  $R_{23}$  method. We estimated the SFR for our samples of galaxies, and studied the luminosity and mass–metallicity relations. The comparison of our local ( $0.04 < z < 0.1$ ) with our higher redshift sample ( $0.3 < z < 0.4$ ) shows that the metallicity, the SFR, and morphology evolve toward lower values of metallicity, higher SFRs, and late–type morphologies for the redshift range  $0.3 < z < 0.4$ . Finally, we find a fundamental plane for field galaxies relating the SFR, gas metallicity, and stellar mass for SF galaxies in the local universe. One of the applications of this plane would be to estimate stellar masses from SFR and metallicity. High redshift data from the literature at redshift  $\sim 0.85$ , 2.2, and 3.5, do not show evidence of evolution in this fundamental plane.

## 1 Introduction

The formation and evolution of galaxies at different cosmological epochs are driven mainly by two linked processes: the star formation history and the metal enrichment. Thus, from

an observational point of view, the star formation rate (SFR), the metallicity, and the stellar mass of the galaxies at different epochs will give us important clues to the evolution of galaxies.

A strong dependence on the SFR and the stellar mass and its evolution with redshift has been found, with the bulk of star formation occurring first in massive galaxies, and later in less massive systems (e.g. [13, 4, 14, 2, 3, 26, 11, 25, 7, 28, 10, 24, 6]).

Metallicity is another important property of galaxies, and its study is crucial for a deep understanding of galaxy formation and evolution, since it is related to the whole past history of the galaxy. Metallicity is a tracer of the fraction of baryonic mass already converted into stars and is sensitive to the metal losses due to stellar winds, supernovae, and active nuclei feedbacks. A detailed description of the different metallicity methods and calibrations are given in [17, 18].

Stellar mass and metallicity are strongly correlated in SF galaxies, with massive galaxies showing higher metallicities than less massive galaxies. This relationship provides essential insight into galaxy formation and evolution. The mass-metallicity ( $M-Z$ ) relation first observed by [21] has been intensively studied ([30, 5, 32, 29, 12, 27], among others), and it is well established by the work of [31] for the local universe ( $z \sim 0.1$ ) using SDSS data. The study of the redshift evolution of the  $M-Z$  relation has provided us with basic information on the cosmic evolution of star formation.

## 2 Data processing and sample selection

We used the SDSS-DR5 spectra from the STARLIGHT database<sup>1</sup>, which were processed with the STARLIGHT spectral synthesis code, developed by Cid Fernandes and collaborators [8, 9, 23, 1]. From the full set of galaxies, we only consider galaxies whose spectra show the  $H\alpha$ ,  $H\beta$ ,  $[N\text{ II}]$ ,  $[O\text{ II}] \lambda 3727$ ,  $[O\text{ III}] \lambda 4959$ ,  $[O\text{ III}] \lambda 5007$ ,  $[O\text{ I}] \lambda 6300$ , and  $[S\text{ II}]$  lines in emission. We selected galaxies with a S/N higher than  $3\sigma$  for the  $H\alpha$ ,  $H\beta$ , and  $[N\text{ II}]$  lines.

To identify any evolution of galaxy parameters or relations, we divided our sample in four redshift intervals as follows:  $0.04 \leq z_0 < 0.1$ ,  $0.1 \leq z_1 < 0.2$ ,  $0.2 \leq z_2 < 0.3$ ,  $0.3 \leq z_3 \leq 0.4$ . The lower limit of  $z_0$  corresponds to an aperture covering fraction of 20%, which is the minimum required to avoid domination of the spectrum by aperture effects. We selected galaxies with an apparent Petrosian  $r$  magnitude of  $14.5 < r < 17.77$  in the redshift samples  $z_0$ ,  $z_1$ , and  $z_2$ , corresponding to the magnitude completeness at these redshifts (see Fig. 1). Galaxies of the  $z_3$  sample have a different completeness range  $16.9 < r < 18.8$ , giving 119 galaxies. We used the  $z_0$  and  $z_1$  sample of galaxies with its respective completeness, but for galaxies of samples  $z_2$  and  $z_3$  we used both those in the completeness range and those out of the completeness range. The reason for this was to improve the galaxy statistics by increasing their number. As we show in the next sections, the main results are similar using galaxies in the magnitude completeness and galaxies of the total sample. Finally, we selected SF galaxies following the criterion in the BPT empirical diagnostic diagram:  $\log[O\text{ III}] \lambda 5007/H\beta \leq 0.61/\{\log([N\text{ II}] / H\alpha) - 0.05\} + 1.3$ . After all these selections, the number of

<sup>1</sup><http://www.starlight.ufsc.br>

galaxies of each redshift bin is reduced to 61921 SF galaxies for  $z_0$ , 27853 for  $z_1$ , 1671 for  $z_2$ , and 67 H II galaxies for  $z_3$ .

### 3 Evolution of the mass–metallicity and luminosity–metallicity relations

In Fig. 1 we show the  $M-Z$  and  $L-Z$  relations for our sample of galaxies. The metallicity decrement for the  $z_3$  redshift sample discussed in our previous articles [17, 18] is also evident.

Our  $z_3$  sample is composed only of spiral galaxies, then our metallicities will be lower than if our sample were composed of a mix of morphological types. In other words, the morphology of the galaxies is crucial in deriving and comparing the metallicity and the  $M-Z$  relation [19].

An additional point is that our samples plotted in Fig. 1 are selected with different magnitude completeness, then, our  $z_3$  redshift sample is more luminous and massive than our local one. This must be taken into account when comparing both  $M-Z$  relations. Unfortunately, our  $z_0$  sample does not have enough galaxies in the same absolute magnitude range of the  $z_3$  sample, making it impossible to generate a local  $M-Z$  relation comparable in luminosity to the  $z_3$  one.

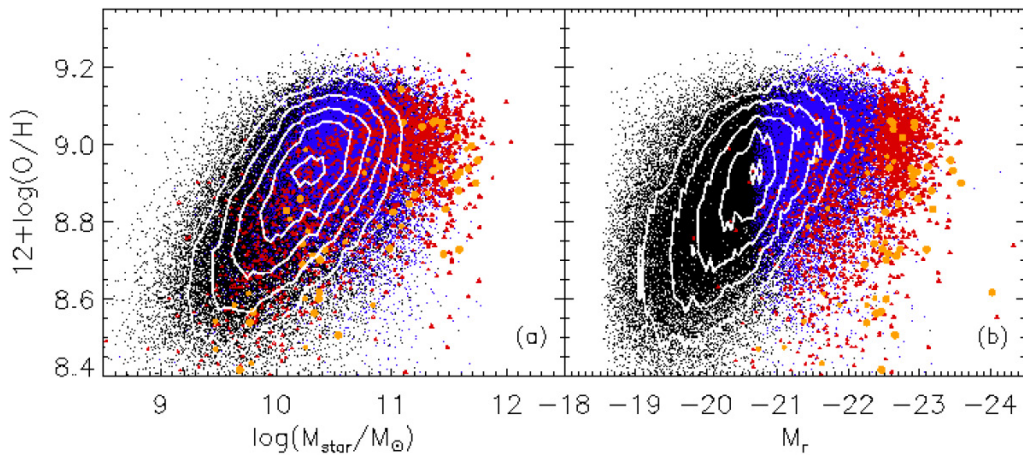


Figure 1: (a) Relation between the stellar mass and  $12 + \log(\text{O}/\text{H})$  ( $M-Z$  relation). (b) Relation between the absolute Petrosian  $r$  magnitude and  $12 + \log(\text{O}/\text{H})$  ( $L-Z$  relation) for our sample of galaxies. The cut observed in (b) for the  $z_1$  sample comes from the  $5577 \text{ \AA}$  sky line (see the text). In both relations, white contours represent from outside to inside, 15, 30, 50, 70, and 90% of the maximum density value of the  $z_0$  redshift sample (black dots) and are only plotted as a visual aid.

## 4 Evolution of the SFR

We estimate the SFR with the  $H\alpha$  emission line flux following the [15] expression:

$$\text{SFR} [M_{\odot} \text{ yr}^{-1}] = 7.9 \times 10^{-42} L(H\alpha) [\text{erg s}^{-1}], \quad (1)$$

where  $L(H\alpha)$  denotes the intrinsic  $H\alpha$  luminosity, and  $H\alpha$  is corrected by dust extinction and underlying stellar absorption. This calibration is derived from evolutionary synthesis models that assume solar metallicity and no dust, and it is valid for a  $T_e = 10^4$  K and a case B recombination

In our sample, galaxies with high SFRs are more abundant at higher redshifts (see Fig. 2), a fact already observed in non biased samples (e.g. [24]). In Fig. 2 a, we show  $12 + \log(O/H)$  against  $\log(\text{SFR})$ . Although our  $z_3$  sample of galaxies is biased to the most luminous and massive galaxies, the observed decrement of  $\sim 0.1$  dex in  $12 + \log(O/H)$  found in [17, 18] is also present. Regarding the  $z_0$  sample of galaxies, there is a clear sequence with galaxies going toward higher values of SFR as metallicity increases. This tendency can be explained from the  $z_0$  sample in the  $M-Z$  relation of Fig. 1, where massive galaxies correspond to the highest metallicity galaxies, and for more massive galaxies, we expect higher SFRs (see Fig. 2). Also, we can slightly appreciate a population of galaxies with higher SFR (see Fig. 2 a). As redshift increases, we appreciate a flattening of the SFR vs.  $12 + \log(O/H)$  relation in Fig. 2 a for galaxies at  $z_2$  and  $z_3$ , with most of the galaxies showing  $\log(\text{SFR})$  between 1 and 2.

In Fig. 2 b, we show the  $\log(M_{\text{star}}/M_{\odot})$  versus  $\log(\text{SFR})$  plot. Galaxies at  $z_0$  show a main sequence, where massive galaxies have higher SFRs. This main sequence was identified by [24], when studying galaxies with redshifts from 0.2 to 1.1, finding that this main sequence moves as a whole to higher SFR as redshift increases [19].

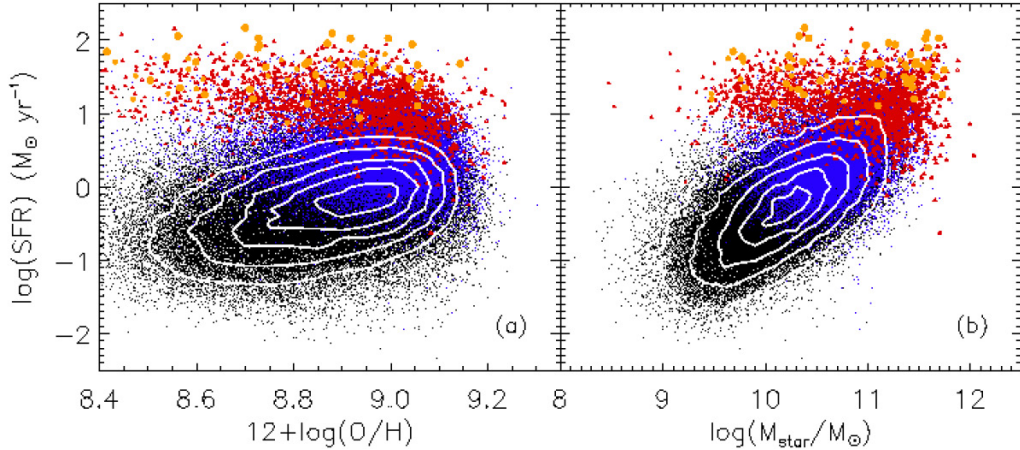


Figure 2: Metallicity and mass versus  $\log(\text{SFR})$ . Contours correspond to the  $z_0$  sample in both plots. White contours represent, from outside to inside, in panel *a*: 15, 30, 50, 70, and 90%, and in panel *b*: 5, 15, 35, 65, and 85% of the maximum density value of the  $z_0$  sample.

Finally, we find a fundamental plane for field galaxies relating the SFR, gas metallicity, and stellar mass for SF galaxies in the local universe. One of the applications of this plane would be to estimate stellar masses from SFR and metallicity. High redshift data from the literature at redshift  $\sim 0.85$ , 2.2, and 3.5, do not show evidence of evolution in this fundamental plane. The results of this study are given in more detail in [20].

## 5 Summary and conclusions

We analyzed the evolution of the  $M-Z$  and  $L-Z$  relations, observing that at higher redshift values, both relations evolve towards lower values of metallicity. We discovered that the flat zone of the  $M-Z$  relation reported by [31] for galaxies with  $\log(M_{\text{star}}/M_{\odot}) > 10.5$ , is mainly constituted by galaxies at  $z > 0.1$  (samples at  $z_1$ ,  $z_2$  and  $z_3$ ). Galaxies at  $z_0$  redshift could be fitted with a linear function. Our  $M-Z$  relation at redshift  $z_3$  is  $\sim 0.2$  dex lower than our local one. We estimated the SFR for our sample of galaxies and analyzed its relation with  $12 + \log(\text{O}/\text{H})$  and  $\log(M_{\text{star}}/M_{\odot})$ , confirming the existence of the MS reported by [24] in the  $\log(\text{SFR})$  vs.  $\log(M_{\text{star}}/M_{\odot})$  plot. Consistently, we found that SFRs increases with redshift.

We have demonstrated the existence of a FP for field SF galaxies in the 3D space formed by the orthogonal coordinate axes  $\log(M_{\text{star}}/M_{\odot})$ ,  $\log(\text{SFR})$  ( $M_{\odot} \text{ yr}^{-1}$ ), and  $12 + \log(\text{O}/\text{H})$ , three of the fundamental parameters of SF galaxies. All these variables have been related previously in pairs as with the  $M-Z$ , metallicity–SFR, and mass–SFR relations, but this is the first time that the correlation for all of them has been quantified.

## References

- [1] Asari, N. V., et al. 2007, MNRAS, 381, 263
- [2] Bauer, A. E., Drory, N., Hill, G. J., & Feulner, G. 2005, ApJ, 621, L89
- [3] Bell, E. F., et al. 2005, ApJ, 625, 23
- [4] Brinchmann, J., & Ellis, R. S. 2000, ApJ, 536, L77
- [5] Brodie, J. P., & Huchra, J. P. 1991, ApJ, 379, 157
- [6] Buat, V., et al. 2008, A&A, 483, 107
- [7] Caputi, K. I., et al. 2006, ApJ, 637, 727
- [8] Cid Fernandes, R., Mateus, A., Sodré, L., Stasińska, G., & Gomes, J.M. 2005, MNRAS, 358, 363
- [9] Cid Fernandes, R., et al. 2007, MNRAS, 375, L16
- [10] Erb, D. K., et al. 2006, ApJ, 644, 813
- [11] Feulner, G., et al. 2005, ApJ, 633, L9
- [12] Garnett, D. R., Shields, G. A., Skillman, E. D., Sagan, S. P., & Dufour, R. J. 1997, ApJ, 489, 36

- [13] Guzmán, R., et al. 1997, *ApJ*, 489, 559
- [14] Juneau, S., et al. 2005, *ApJ*, 619, L135
- [15] Kennicutt, R. C. 1998, *ARA&A*, 36, 189
- [16] Lamareille, F., et al. 2009, *A&A*, 495, 53
- [17] Lara-López, M. A., et al. 2009a, *A&A*, 493, L5
- [18] Lara-López, M. A., et al. 2009b, *A&A*, 505, 529
- [19] Lara-López, M. A., et al. 2010a, *A&A*, 519, A31
- [20] Lara-López, M. A., et al. 2010b, *A&A*, 521, L53
- [21] Lequeux, J., Peimbert, M., Rayo, J. F., Serrano, A., & Torres-Peimbert, S. 1979, *A&A*, 80, 155
- [22] Liang, Y. C., et al. 2006, *ApJ*, 652, 257
- [23] Mateus, A., et al. 2006, *MNRAS*, 370, 721
- [24] Noeske, K. G., et al. 2007, *ApJ*, 660, L43
- [25] Papovich, C., et al. 2006, *ApJ*, 640, 92
- [26] Pérez-González, P. G., et al. 2005, *ApJ*, 630, 82
- [27] Pilyugin, L. S., & Ferrini, F. 2000, *A&A*, 358, 72
- [28] Reddy, N. A., et al. 2006, *ApJ*, 644, 792
- [29] Richer, M. G., & McCall, M. L. 1995, *ApJ*, 445, 642
- [30] Skillman, E. D., & Kennicutt, R. C., Jr., & Hodge, P. W. 1989, *ApJ*, 347, 875
- [31] Tremonti, C. A., et al. 2004, *ApJ*, 613, 898
- [32] Zaritsky, D., Kennicutt, R. C., & Huchra, J. P. 1994, *ApJ*, 420, 87